Environmental Science
Atmospheres

Solar radiation

Metabolism

Gas reagent

Air pollution

Interaction
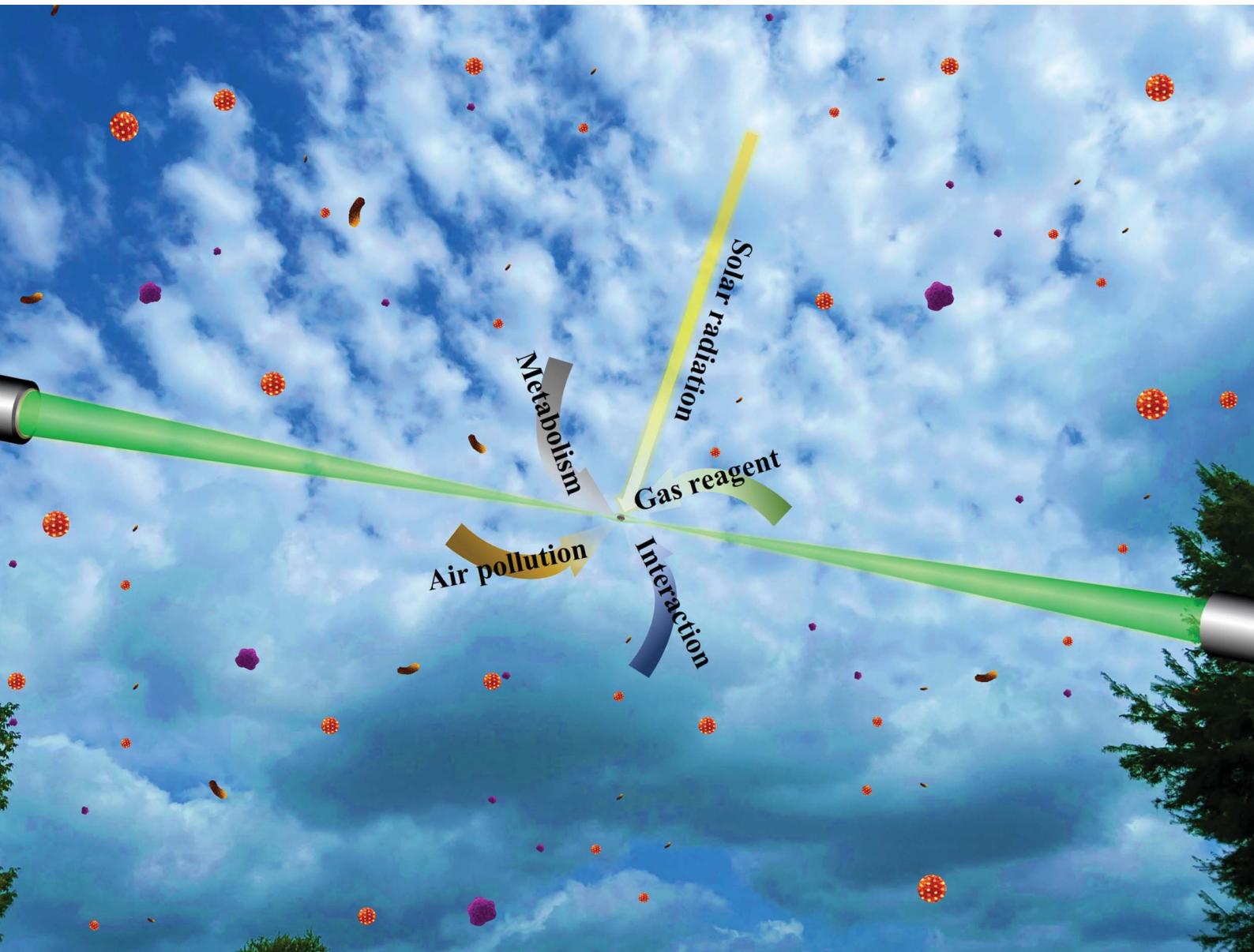
PAPER
Yukai Ai *et al.*
Characterization of single fungal aerosol particles in a reactive atmospheric environment using time-resolved optical trapping-Raman spectroscopy (OT-RS)

Check for updates

Characterization of single fungal aerosol particles in a reactive atmospheric environment using time-resolved optical trapping-Raman spectroscopy (OT-RS)

Yukai Ai, [ID] [a] Chuji Wang,*[a] Yong-Le Pan [ID] [b] and Gorden Videen[b]

We applied a time-resolved, optical trapping-Raman spectroscopy (OT-RS) technique to characterize single, trapped bioaerosol particles under well-controlled reactive conditions that mimic the native state of particles in the atmosphere. We measured Raman spectra of seven different fungus samples using an OT-RS system, in which single fungal aerosol particles of tens of microns in size are trapped without photo-damage while relative humidity and ozone concentration around the particle are well controlled. We initially obtained Raman spectral fingerprints of seven different single-trapped fungal aerosol particles in air. We then measured time-resolved Raman spectra of the fungal aerosol particles trapped in air over a period of 40 minutes and characterized the temporal behavior of the trapped particles in terms of Raman band structure and intensity. We also measured time-resolved Raman spectra of the fungal aerosol particles exposed to ozone in a controlled concentration and relative humidity and compared the spectral features with those obtained when the single fungal aerosol particles were exposed to air. Results show that we not only observed time variations of the physical and chemical properties of single-trapped particles, but also specified several individual chemical function groups such as lipids and proteins that undergo chemical reactions with ozone. This work demonstrated that OT-RS is a powerful technology for characterization of physical, chemical, and biological properties of single bioaerosol particles in simulated atmospheric conditions and for potential detection of single bioaerosol particles in the atmosphere using Raman spectral fingerprints.

Environmental significance

New technologies for characterization and detection of bioaerosols are essential for modelling airborne transmission, risk estimate, and better understanding of bioaerosol properties and their temporal evolution in the atmosphere. In current laboratory and field studies, aerosol samples are either collectively or individually placed on a substrate or in a sample holder for subsequent measurements that may experience signal interference from particle-surface contamination or modification. Here we present a time-resolved, optical trapping, single-particle technology and apply it to characterize fungal aerosol particles that are freely suspended in a reactive atmospheric environment. This work demonstrates a technology platform for single airborne particle studies, such as formation, loss, and surface chemistry.

1 Introduction

Characterization and detection of bioaerosol particles in the atmosphere is of significance in indoor and outdoor air-quality monitoring,[1,2] surface decontamination,[3] food processing and storage,[4,5] infectious diseases control,[6] and biodefense in special situations.[7] Atmospheric air contains a wide variety of aerosols including bioaerosols that affect human health and the climate. It is reported that aerosolized fungi, such as *Aspergillus* species and *Penicillium* species, have been correlated to lung diseases in many cases, as indoor air quality can be adversely affected by the fungal contamination in a damp building.[8] As fungal aerosols develop, they release toxic compounds, which can cause various respiratory allergies or diseases, such as, asthma, rhinitis, and hypersensitivity pneumonitis.[8,9] Moreover, aerosolized fungi can change with surrounding environmental conditions such as relative humidity (RH), air pollutants, UV radiation, and reactive molecules such as ozone (O_3).[10–12] In addition, food contamination caused by bioaerosols impacts public health.[5] For example, *Aspergillus* species is a main contaminant in food chains. Biotoxins, such as aflatoxins, ochratoxins, patulin, *etc.*, produced by the *Aspergillus* species can cause diseases and even death in humans and other

[a]*Department of Physics and Astronomy, Mississippi State University, Starkville, MS, 39759, USA. E-mail: cw175@msstate.edu*

[b]*CCDC-U.S. Army Research Laboratory, 2800 Powder Mill Road, Adelphi, Maryland, 20783, USA*

© 2022 The Author(s). Published by the Royal Society of Chemistry

Environ. Sci.: Atmos., 2022, **2**, 591–600 | **591**

animals.[4] Furthermore, bioaerosols generate a potential threat to national security as biological warfare agents may be aerosolized and released into the atmosphere.[7,13] Therefore, characterization and detection of bioaerosol particles, especially when they are presented in the atmosphere where aerosol particles are often in a low concentration and exposed to possible chemical reactants, has become increasingly important.

Many techniques have been developed and applied for the detection and characterization of atmospheric bioaerosols. Generally, the techniques can be grouped into three categories: (1) optical microscopy, scanning electron microscopy, and transmission electron microscopy, which are commonly utilized for the characterization of physical properties, such as particle's size, shape, and structure,[14,15] (2) X-ray spectrometry, laser-induced breakdown spectroscopy, and mass spectrometry, *etc.*, which are typically used for analyzing elemental compositions,[16–18] and (3) Raman spectroscopy, laser-induced fluorescence, and quantitative polymerase chain reaction (qPCR), which are used for the characterization of chemical and biological properties.[19–23] However, these traditional methods either require collection of a relatively large volume of samples or the use of a substrate or a cuvette to hold samples for subsequent measurements.[24] In many cases, the sample collection and processing are time consuming. More importantly, particle surface properties may be modified during the sampling process and measurements may be optically interfered by the surface of the substrate.[25,26] Single-particle measurements by scanning Raman spectra of single pollen grains placed on a substrate have been reported,[27,28] but for bioaerosols, properties can dramatically change when they are released into air.[24,29–31] Chemical properties may change through reactions with atmospheric molecules and air pollutants. For example, the structure of lipids, proteins, and polysaccharides in some bioaerosols can be modified when the bioaerosols are exposed in an environment containing O_3,[32] and even new chemicals may be produced through O_3 oxidation processes.[33] As a result, the intrinsic value and viability of the organisms in the bioaerosol particles are influenced, and subsequently molecules fingerprints or signatures that are used for characterization and detection (*e.g.* in fluorescence, Raman spectra, and PCR) are affected. Therefore, in order to characterize properties of atmospheric bioaerosols accurately, it is better to study them under well-controlled environmental conditions that are close to their native atmospheric state, in which individual particles should be suspended in air with no surface interactions with surrounding particles or solid surfaces of the sample holder.

One way to mimic the native state of atmospheric aerosols is to levitate single particles in air or in a controlled reactive environment.[34,35] There are three main techniques to levitate or trap a single particle: electrodynamic levitation, such as double ring electrodynamic balancing (EDB) and quadrupole linear trapping, acoustic levitation, and optical trapping (OT). The EDB technique requires charging particles.[36] Acoustic levitation can levitate a single particle in an

acoustic interference field, which is mainly suitable for particles of large size, *e.g.* millimeters,[37] thus it is not useful for the investigation of atmospheric aerosol or bioaerosol particles that are typically from tens of nanometers to tens of microns.

Particle levitation using the light force was first demonstrated by Ashkin in the 1970s.[38] Later the idea was used to achieve laser cooling atoms by Chu who received the Nobel Prize in physics in 1997. In 2018, Ashkin also received the Nobel Prize in physics for his contribution to the OT technology, which now has ever expanding impacts in diverse fields, such as materials, physics, chemistry, life sciences, and atmospheric sciences.[38–44] Over the last several decades, developments of OT technologies for particle trapping and manipulation have advanced significantly. Optically trapping a single particle in air involves two types of light forces, radiation-pressure force (RPF) and photophoretic force (PPF). The RPF is generally created by a tightly focused laser beam to trap a non-absorbing particle. The PPF is formed by the photopheresis as a result of differences in the particle's surface temperature and the surface thermal accommodation coefficient, mainly applied to trap the strongly absorbing particle. Now we can use a universal optical trap (UOT) which combines RPF and PPF, in most cases, to trap single particles of arbitrary size, morphology, and material property in air or in different media.[26,45] Once a particle is trapped, several advanced laser spectroscopy and optical techniques can be integrated, individually or in combination, for subsequent observation and measurement of physical and chemical properties of the particle. These techniques include Raman spectroscopy, cavity-ringdown spectroscopy, elastic light scattering, and digital imaging. Details of recent developments and advancements of optical trapping, manipulations, and measurements of single particles in air can be seen in recent reviews.[46–49] Very recently, changes in chemical properties of a single pollen fragment exposed to an O_3 environment are monitored by OT-RS.[32]

In this work, we measured single particles of seven different fungus materials using the time-resolved OT-RS. Firstly, we characterized Raman spectra of a single fungal aerosol particle optically trapped in air. Secondly, we measured the time evolution of OT-RS from seven different samples when they are exposed to ambient lab air or to O_3. We compared their Raman spectral features in terms of Raman peaks, peak intensity, relative peak intensity ratio, and their time variations over a period of 40 minutes. Thirdly, based on changes in the spectra, we investigated the possible chemical or biological reactions of a single fungal aerosol particle with O_3. Fourth, we decoupled the overlapped Raman bands in the long-Raman-shift region (around 3000 cm^{-1}) into individual Raman peaks and assigned them to specific chemical function groups. We identified several chemical function groups such as lipids and proteins that participated in chemical reactions. To the best of our knowledge, this is the first report on characterization of single bioaerosol particles that are optically trapped in a controlled reactive environment, with no particle damage.

2 Methodology

2.1 Experimental setup

Fig. 1 shows key components of the OT-RS system. A linearly polarized, continuous-wave laser at 532 nm was used as the trapping laser source and the power was set at 1500 mW for the experiment. The laser beam was split into two parts with the same intensity by the beam splitter. The two laser beams formed two counter-propagating hollow beams by a pair of axicons and two microscope objectives ($\times$50, numerical aperture (N.A.) = 0.55). A UOT was formed in an airtight reaction chamber and a hollow trapping region (an optical cage) is formed between the two foci of the microscope objectives. In this case, the size of the trapping region can be adjusted by precisely tuning the separation distance between the two foci. Experimentally, the separation distance was set from several microns to $\sim$100 μm, depending on individual particle size and material properties. A single particle was trapped in the hollow trapping region, where the trapping beams did not directly touch the surface of the particle. In this way, no photo-induced chemical damage occurs to the particle once it is trapped inside the UOT, except that some mass loss may occur due to thermal evaporation of surface materials (see Section 3.2). However, when particles are entering the UOT during the sample introduction, they may be overheated by the trapping beams and thermally decomposed when the trapping beams are strong, or the sample material is thermally sensitive.[32]

The Raman signal was excited by the scattered light of the trapping beams. Raman signals were collected by the third microscope objective ($\times$20, N.A. = 0.42) to a spectrograph (Princeton Instrument, Action SP2300) and recorded by an electron-multiplying charge-coupled device (EMCCD, Princeton, ProEM1600). In addition, a camera (Point Grey, GS3-U3-32S4C-C) that was integrated in the setup captured images of the trapped particle and monitored the particle during the entire trapping period in real time.[50] A blue LED was used as the light source illuminating the particle for imaging. A short-pass filter ($\lambda_{cut\ off}$ = 500 nm) was placed in the front of the camera to block the 532 nm scattering light of the particle. In this setting, the image that was captured by the camera showed the size and

shape of the particle, while the time-resolved Raman spectra tracked changes in chemical compositions of the particle, simultaneously. Compared to the setup in the previous study,[32] the part for the introduction of chemical reagents was further developed in this work. As shown in Fig. 1, two sensors were inserted into the chamber to monitor RH and temperature inside of the chamber. O_3 was generated by photolysis of oxygen (O_2) through the illumination of the ultraviolet light produced by a mercury lamp. The mercury lamp was placed inside a home-built device. The high-purity O_2 (99.99%) flowed into the chamber at a controlled flow rate. The O_3 concentration was controlled in the range of 10–1200 parts per million (ppm) by adjusting the portion of the lamp inserted into the chamber. Adjacent to the mercury lamp was a homemade humidifier that was used to control RH in the reaction chamber. The RH of the introduced chemical gas-flow was controlled in the range of 20–40%. The water vapor was produced by an inversely mounted ultrasonic disc, then carried by flowing O_2 or O_3. All flow gases passed through the O_3 sensor, which read the O_3 concentration. In the experiment, particles were dusted directly to the chamber through a small open hole on the top of the chamber. In this case, if no O_3 or other chemical reagent was introduced during the experiment, the air condition inside the chamber was the same as the ambient lab air. If the O_3 was introduced, the O_3 passed through the trapped particle then was released to an exhaust sucking system *via* the open hole.

2.2 Samples

Seven aerosol samples used in this study are fungi: *Aspergillus fumigatus*, *Aspergillus versicolor*, *Cladosporium herbarum*, *Paecilomyces variotii*, *Penicillium camembertii*, *Penicillium chrysogenum*, and *Penicillium digitatum*. They were purchased from the Greer Lab where the samples were grown in a media of enriched trypticase then killed by acetone. The samples are dried powders of millimetres in size and in black or dark grey color. In the experiment, the particle powders were further ground to submicron to tens of microns in size. As this study focuses on characterization and chemical reaction of single particles, instead of sensing the atmospheric aerosols, results are not related to the aerosol concentration in sampling and to other environmental interferences. No sample preparation procedure or further purification was conducted. The ground samples were directly dusted into the reaction chamber.

3 Results and discussion

3.1 Single-particle Raman spectra of seven fungus samples

Fig. 2 shows the single-particle Raman spectra of the seven different fungus samples. These spectra were obtained in the first minute after the particle was trapped in the ambient lab air in the reaction chamber. The temperature inside the chamber is same as the lab temperature which is controlled around 20 °C and the RH is controlled around 30%. Each spectrum was obtained by using an interrogation time of 60 seconds. The grating used in the spectrograph is 600 groves per mm, which sufficed a survey of characteristic Raman
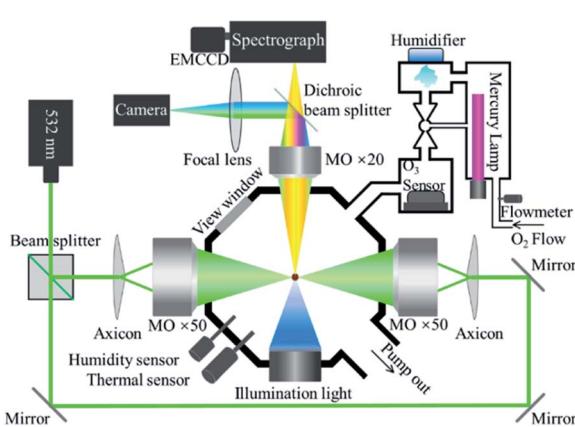

Fig. 1 Schematic of the experimental setup of the OT-RS system.

© 2022 The Author(s). Published by the Royal Society of Chemistry

Environ. Sci.: Atmos., 2022, **2**, 591–600 | **593**
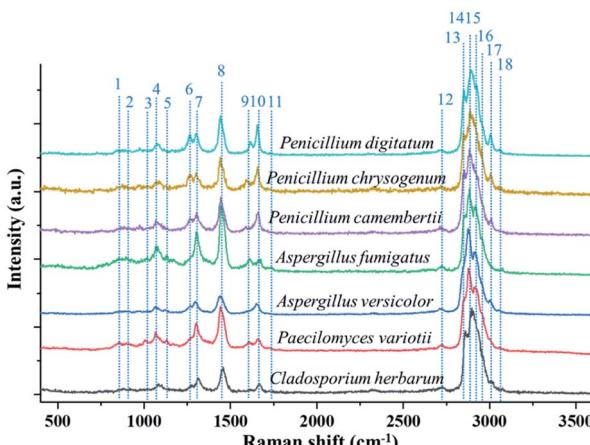
Fig. 2 Single-particle Raman spectra of seven different fungus samples optically trapped in a reaction chamber under controlled environment.

bands. Most bioaerosol particles have strong fluorescence emissions, which can generate a strong interference in their measured Raman spectra and can even engulf relatively weak Raman bands. Even though the Raman spectra of a single trapped particle are free from the interference from the substrate, the single particle measured spectra can still be affected by the fluorescence interference. Some early works showed that the single-particle Raman spectra, which were obtained by using an EDB device, were strongly influenced by fluorescence.[51] In 2015, Wang *et al.* reported measurements of Raman spectra of single bioaerosol (pollens and grass spores) particles photophoretically trapped in air. The results showed that five barely noticeable Raman bands were observed in the CH stretching region around 3000 cm^{-1}.[41] Despite that some Raman bands in the short Raman-shift region were resolved in that work, the baseline fluorescence was noisy and strong, and

many Raman peaks were severely interfered by fluorescence. Recently, Gong *et al.* reported the fluorescence-free Raman spectra of fluorescence-dye-coated spheres optically trapped in air.[40] In that study, the trapped single particles experienced a photobleaching process, and the fluorescence was cleaned within several seconds after the particle was trapped. Later, they reported the fluorescence-free Raman spectra of single pollen fragments by utilizing the same system.[26] In that case, the UOT formed by the counter-propagating hollow beams effectively reduced the fluorescence. In the present study, the Raman spectra, shown in Fig. 2, captured by the OT-RS system are also fluorescence-free. The single-particle Raman spectra in Fig. 2 are used as a baseline of the Raman spectral finger-prints for the seven sample materials, and this baseline will be compared with the subsequent time-resolved Raman spectra obtained when the samples are exposed to air and to O_3 under controlled conditions.

The typical Raman bands from different fungus samples are listed in Table 1. As shown in Fig. 2, the seven different fungi have similar Raman bands. For example, all the samples show the Raman band at 1080 cm^{-1}, which comes from the C–O–C glycosidic link or the C–C skeletal stretch.[26] The Raman shift in the region from 1220 cm^{-1} to 1350 cm^{-1} is from the amide III band, which is shown in the spectra of all seven materials.[52] The band around 1450 cm^{-1} is related to lipids, proteins, or the CH_2 deformation. The band at 1660 cm^{-1}, which comes from the amide I group, is also found in all the samples.[53] Besides these common bands, some bands representing specific chemical properties are also identified in terms of some types of fungi. The band around 1131 cm^{-1} from the palmitic acid is found in the *Aspergillus* type of fungus.[52] Only *Penicillium* type shows the band around 1267 cm^{-1}, which comes from the CH stretching (lipids in normal tissue).[52] The spectral peak marked as no. 11 at 1750 cm^{-1} comes from C=O or lipids, indicating the unique composition of *Aspergillus* species.[52] Additionally, Fig. 2 shows

Table 1 Assignments of the measured Raman bands from the single-trapped fungal aerosol particles

Peak no.	Bands (cm^{-1})	Assignment	Ref.
1	840	Tyrosine	52
2	892	C–O–C backbone, C–C skeletal stretches	53
3	1032	Phenylalanine	52
4	1080	C–O–C glycosidic link, C–C skeletal stretches	26
5	1131	Palmitic acid	52
6	1267	CH (lipid in normal tissue), triacylglycerol	52
			54
7	1298	CH_2 deformation	53
8	1450	Lipid/protein, CH deformation	52
9	1610	Cytosine	52
10	1660	Amide I	53
11	1750	C=O, lipids	52
12	2739	Stretching vibrations of CH	52
13	2855	CH_2 symmetric stretch of lipids	52
14	2878	CH_2 symmetric stretch of lipids	52
15	2915	CH_2 stretch lipids and proteins	52
16	2960	Out-of-plane chain end antisymmetric CH_3 stretch band	52
17	3008	ν_{as}(=CH), lipids, fatty acids	52
18	3059	(C=CH) aromatic stretching	53

that all the spectra have a large composite peak (overlapped or partially overlapped band package) between 2700 cm^{-1} and 3100 cm^{-1}. This band package is formed by several Raman bands, and most of them are from the CH stretching. For example, band no. 12, which is located at 2739 cm^{-1}, comes from CH-stretching vibrations. Band no. 13 and 14, at 2855 cm^{-1} and 2878 cm^{-1} respectively, are from the CH$_2$ symmetric stretch of lipids. Peak no. 15 at 2915 cm^{-1} denotes the components of proteins. Peak no. 16 at 2960 cm^{-1} is the out-of-plane, chain-end, antisymmetric CH$_3$ stretch band. Peak no. 17, around 3008 cm^{-1}, is from lipids and fatty acids.[52] In the present work, the sharp peaks in the short-wavenumber region and the overlapped band package around 3000 cm^{-1} were obtained in a high-spectral-resolution setting. Using the deconvolution method to decompose the overlapped band package around 3000 cm^{-1}, more detailed information on spectral changes, temporal evolution, and chemical reaction can be revealed (see Section 3.4).

3.2 Temporal evolution of single-particle Raman spectra

The OT-RS system can not only characterize chemical properties of the trapped particles, but also monitor the temporal evolution of the particle's physical properties, such as the particle's size and morphology *via* the real-time imaging system. Theoretically, how long a particle can be trapped depends on many factors.[26] Among seven fungus samples, four of them, which are *Cladosporium herbarum*, *Penicillium camembertii*, *Aspergillus fumigatus*, *Paecilomyces variotii*, could be stably trapped for more than 30 minutes, while the other three samples could only

be trapped for several minutes. Fig. 3(a) and (c) show the temporal evolution of the spectra of single *Penicillium camembertii* and *Paecilomyces variotii* particles trapped in the ambient lab air. The size of the two trapped fungal aerosol particles is about 1.5 μm and 2.0 μm respectively. In the experiment, changes in experimental settings, including variations of the trapping laser power, can be monitored by the intensity of the nitrogen band at 2331 cm^{-1}, which is from the nitrogen in the ambient lab air. In Fig. 3(a), the peak intensity of all bands decreases, while the intensity of the nitrogen band at 2331 cm^{-1} is invariant. The structures of the Raman bands around 2700–3100 cm^{-1} show some small variations, in addition to the decreased intensity. Fig. 3(b) shows intensity changes of the five Raman bands shown in Fig. 3(a) over 40 minutes, and each point was averaged over three measurements. Except for the nitrogen band, the other four bands decrease in intensity. This intensity decrease is due to the mass loss of the trapped particle resulting from thermal decomposition or evaporation of chemicals on the surface of the particle, resulting from the long period of trapping.[13] The mass loss can be estimated by the particle image. As shown in the inset image, the size of the particle in first minute is about 1.92 μm, and in 40 minutes is about 1.65 μm. Therefore the mass loss is calculated to be ∼26.13% by the ratio of the volume. Similarly, Fig. 3(c) shows the temporal evolution of the Raman spectra of a single trapped *Paecilomyces variotii* particle in lab air. The time-evolution of the band intensity that is averaged over three measurements is shown in Fig. 3(d). The intensity of three bands decreases while the intensity of the band at 1610 cm^{-1} increases slightly. This
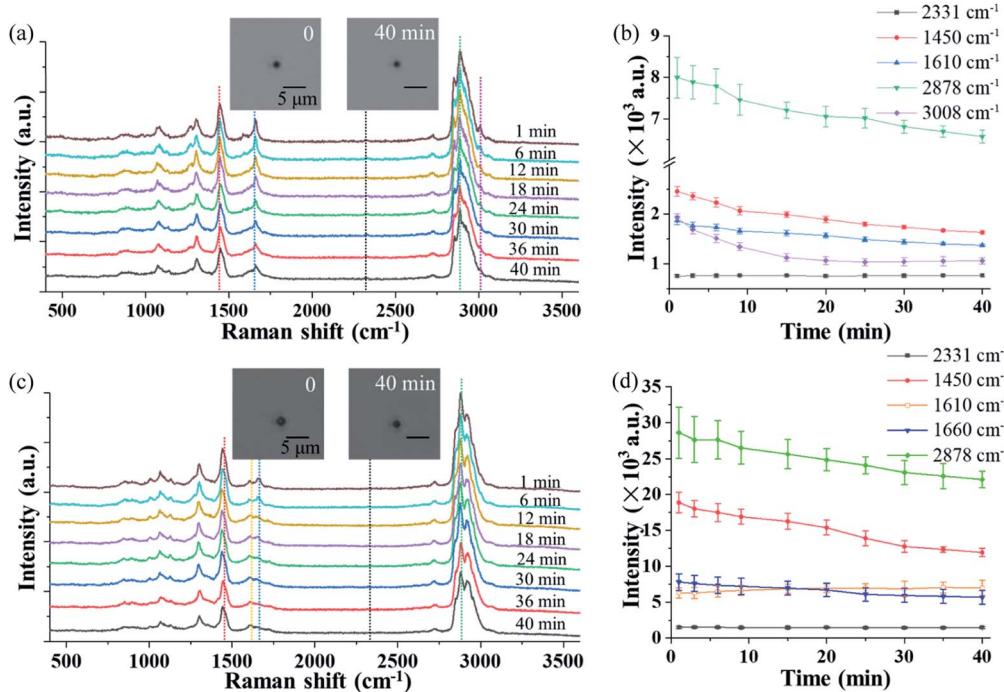
Fig. 3 (a) The temporal evolution of the Raman spectra of single trapped *Penicillium camembertii* particles in lab air; (b) time variations of the peak intensity of representative Raman peaks; (c) and (d) are the temporal evolution of the spectra and the intensity of single trapped *Paecilomyces variotii* particles in lab air. The insets in (a) and (c) are the captured images of the trapped particles at different times.

© 2022 The Author(s). Published by the Royal Society of Chemistry

Environ. Sci.: Atmos., 2022, **2**, 591–600 | **595**

different spectral feature differentiates *Paecilomyces variotii* fungus from *Penicillium camembertii* fungus. The decrease of the Raman band is also due to the mass loss. The size of the particle in first minute is about 2.43 μm, and in 40 minutes is about 2.19 μm, the mass loss for *Paecilomyces variotii* fungus can be estimated to be ~27.04%.

3.3 Raman spectra in the short-wavenumber region from chemical reaction in single trapped particles

Fig. 4(a) shows the time evolution of the Raman spectra in the short-wavenumber region of 400–2000 cm^{-1} of a single trapped *Penicillium camembertii* particle exposed to O_3 at 800 ppm. The RH in the reaction chamber was controlled at 30% over the measurement period. The Raman spectra have a higher spectral resolution than that in Fig. 2 and 3, as the grating was set to 1200 g mm^{-1}. The spectral integration time was 60 seconds. The Raman band at 1550 cm^{-1} from O_2 keeps the same level of intensity over 40 minutes, which indicates the O_2 concentration was constant in the reaction chamber. This also indicates that the O_3 concentration was constant during the observation period.

However, intensity features of other Raman bands shown in Fig. 4(a) are different. The intensity of most Raman bands, such as bands at 968 cm^{-1}, 1267 cm^{-1}, and 1660 cm^{-1}, gradually decrease, but a band at 1131 cm^{-1} gradually increase over the period of 40 minutes. Fig. 4(b) shows the time variations of the bands identified in Fig. 4(a), and each point was averaged over three measurements. As shown in Fig. 4(b), the time-variation feature of the Raman bands of the particle exposed to O_3 is completely different from when the particle is exposed to air, as shown in Fig. 3. This observation indicates that the trapped particle underwent an O_3 chemical reaction.

The intensity of the peak at 1660 cm^{-1} decreased rapidly after the particle was trapped. The peaks at 968 cm^{-1} and 1267 cm^{-1}, which are lipids and triacylglycerol, respectively, also decreased right after the particle was trapped. This decrease may indicate a change of the fatty acid. For instance, the decreasing peak at 968 cm^{-1} is from elaidic acid. The gradual disappearance of the Raman band at 1267 cm^{-1}, which is from the C–C stretching vibration, can be explained as the break of the carbon chain.[54] The disappearance of these two

peaks can be further validated by the rising peak at 1131 cm^{-1}, which results from the formation of palmitic acid. In general, the fatty acid exists in the form of multiple polymorphs and polytypes, depending on the temperature, pressure, and crystallization condition. Under different conditions, one form of fatty acid may transform to another form with better chain packing to maintain the highest stability.[54,55] In addition to the change at 1660 cm^{-1}, which is from the mass loss, the changes of Raman bands at 968 cm^{-1} and 1267 cm^{-1} are also due to the mass loss of the particle. No significant change is observed at a higher airflow rate and higher O_2 concentration. This indicates that the mass loss is determined by the intrinsic chemical property of the particle rather by the airflow rate and O_2 concentration.

In comparison to the change of the Raman bands caused by the mass loss, significant changes in several Raman bands are found after the introduction of O_3. The peak at 840 cm^{-1}, which relates to tyrosine, decreased in the O_3 environment, while it remained invariant when the particle was trapped in air. The decrease is caused by the reaction of tyrosine with O_3. It was reported that tyrosine is sensitive to O_3, and it is oxidized by O_3 and converted into aspartic acid.[56] As shown in Fig. 4(a), a small peak package in the region of 1700–1750 cm^{-1} started to increase after 15 minutes. The growth of this band package suggests the formation of aspartic acid. Another peak at 1005 cm^{-1} emerged after 10 minutes when O_3 was introduced. This peak is related to phenylalanine,[57] which is probably a product from the lipid oxidation. Moreover, one peak at 1730 cm^{-1}, which is a small peak package, comes from ν(C=O), suggesting the formation of carbonyl products.[32] These observations show that the particle properties are modified *via* the O_3 oxidation process.

Fig. 5(a) and (b) show the high-resolution Raman spectra in the long-wavenumber region around 3000 cm^{-1} of the single trapped particle exposed to O_3 at 800 ppm. The spectra were obtained from the same particle as that in Fig. 4. Even though the grating was set to 1200 g mm^{-1} for high-resolution spectra, the band package in this region cannot be resolved. The spectrum in Fig. 5(a) was captured in the first minute after the particle was trapped in O_3, and the spectrum in Fig. 5(b) was obtained after exposure to O_3 for 40 minutes.
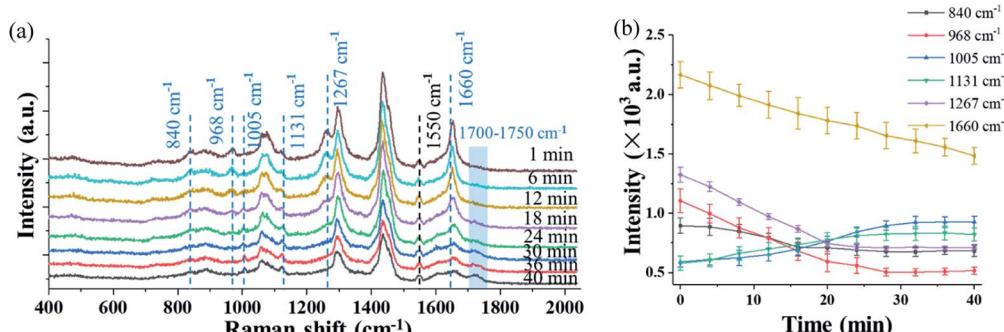

Fig. 4 (a) The time-evolution of the Raman spectra of a single trapped *Penicillium camembertii* particle exposed to O_3 in the wavenumber region of 400–2000 cm^{-1}; (b) time-variations of the intensity of the characteristic Raman bands over a period of 40 minutes.
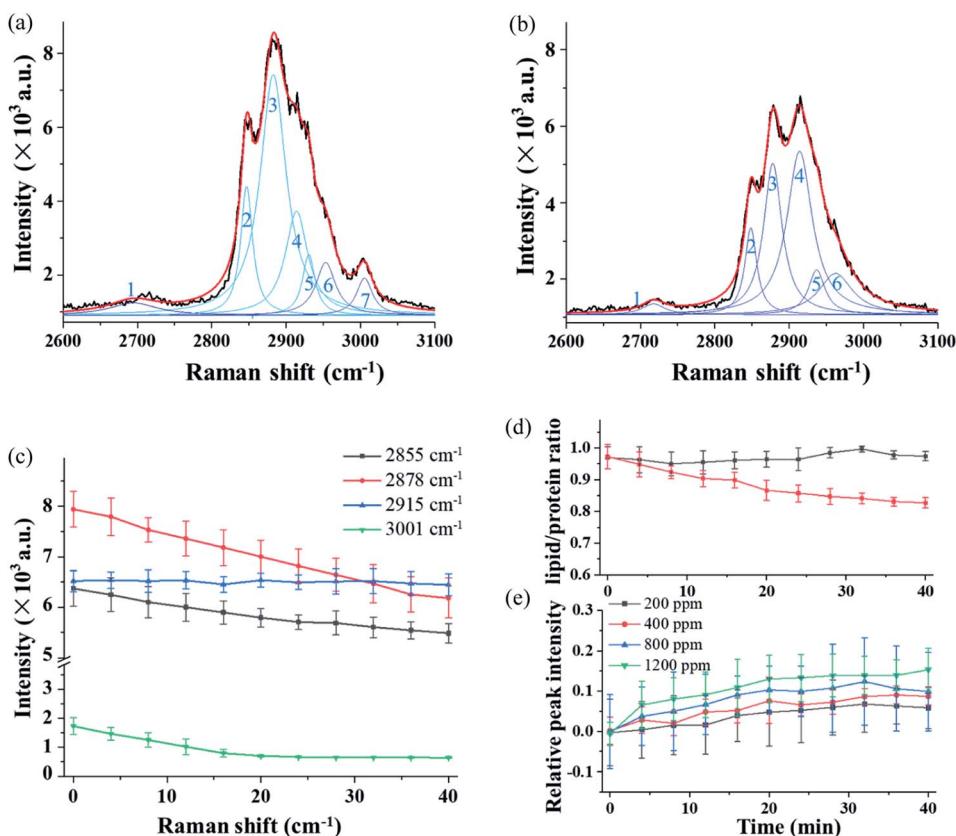
Fig. 5 The Raman spectra in the long-wavenumber region around 3000 cm^{-1} of a single trapped *Penicillium camembertii* particle exposed to O$_3$ in (a) the first minute and (b) after 40 minutes: the overlapped band packages (red line) are deconvoluted to seven individual peaks (blue lines) numbered 1 to 7; (c) the peak intensity changes for the four Raman bands over the 40 minutes of chemical reaction with O$_3$; (d) lipid/protein ratios represented by the ratios of peak (2855 cm^{-1})/peak (2915 cm^{-1}) under different conditions; (e) the intensity change of the peak at 2915 cm^{-1} in different ozone concentrations.

3.4 Raman spectra in the wavenumber region around 3000 cm^{-1} from chemical reaction in single trapped particles

In order to obtain more detailed information from this overlapped band package, the spectra in Fig. 5(a) and (b) are decomposed using the deconvolution method, and seven individual peaks, numbered 1 to 7, are identified, and each of them is assigned to a specific chemical function group. Compared to the spectrum in Fig. 5(a), the spectrum captured after 40 minutes of exposure shows a significant change in both structure and intensity features, which is due to the chemical reaction of the particle with O$_3$.

Fig. 5(c) illustrates time variations of the four selected Raman bands over a period of 40 minutes and each point was averaged over three measurements. In Fig. 5(c), the intensity of the peak at 2878 cm^{-1} decreases rapidly after the particle was trapped. This is mainly caused by the mass loss of the particle resulting from the thermal decomposition over the long trapping period. In contrast, the change of peak at 2915 cm^{-1} shows a completely opposite trend. Compared to the decreasing peaks, this peak intensity increases. The peak comes from the CH$_2$ stretch of lipids and proteins. This result suggests that the structure of the protein or lipids is affected by the reaction with O$_3$. The lipid band has a higher level of energy (2855 cm^{-1}) than

the protein band (2915 cm^{-1}). Therefore, the change of the CH band is an indicator reflecting the lipid–protein ratio in the trapped particle.[54,55] Fig. 5(d) shows the time variation of the lipid–protein ratio, which is represented by the intensity ratio of the two Raman bands at 2855 cm^{-1} and 2915 cm^{-1}. The curve in black squares in Fig. 5 (d) is from the single particle trapped in air. The flat curve shows the lipid–protein ratio stays unchanged when the particle is exposed to air during the 40 minutes. However, the lipid–protein ratio decreases rapidly when the particle is trapped in the O$_3$ environment. In this case, the decreasing trend of the ratio indicates that the lipids in the fungal aerosol particle are more sensitive to O$_3$ than proteins. Furthermore, the change in the Raman spectra in Fig. 4 and 5 also indicates that O$_3$ not only modified the molecular structure but also generated new chemicals *via* interaction with proteins and lipids in the particle.

We also investigated the reaction of the particle with O$_3$ in different concentrations. The Raman band at 2915 cm^{-1} was used to show reactions at deferent O$_3$ concentrations. The results are shown in Fig. 5(e), in which each data point was averaged over three measurements. In the experiment, the O$_3$ concentration was varied from 200 ppm, 400 ppm, 800 ppm, to 1200 ppm. The results show that the changing rate of the band

© 2022 The Author(s). Published by the Royal Society of Chemistry

Environ. Sci.: Atmos., 2022, **2**, 591–600 | **597**

intensity is affected by the O_3 concentration. With a higher concentration of O_3, the changing rate of the peak at 2915 cm^{-1} becomes higher. Note that the data shown in Fig. 5(e) shows the increasing rate that is normalized by having the change from the mass loss during the long trapping period subtracted.

5 Conclusion

We measured time-resolved, single-particle Raman spectra of seven different fungus materials using the OT-RS technique. The time-resolved Raman spectra obtained when the trapped particles were exposed to the ambient lab air are used as the baseline for comparison to the spectra when the particles were exposed to O_3 under controlled O_3 concentration and RH. The baseline spectra show a uniform decrease in the peak intensity of all Raman bands, which means no photo-induced chemical damage and the peak intensity decrease is due to the mass loss of the trapped particle over the long period of observation. The features of the Raman spectra measured when the trapped fungal aerosol particles were exposed to O_3 are completely different in terms of changes in the Raman-band intensity, presence of new bands, and/or band structures. These results show that chemical reactions of single, trapped fungal aerosol particles with O_3 occurred and can be monitored by their time-resolved single-particle Raman spectra. Furthermore, the high-resolution of the spectra offers more detailed information on the specific chemical-function groups that participated in the reaction. For instance, the change of the lipid–protein ratio in the seven fungus materials over the 40 minutes of reaction was obtained from the time-resolved Raman spectra. This study demonstrates that OT-RS is a powerful, emerging technique for the study of single-particle loss, formation, and chemical reaction in its near-native state. The technology, with further development, can potentially be used for characterization and detection of atmospheric bioaerosols without using a sample substrate and the conventional sample handling and processing.

Conflicts of interest

There are no conflicts to declare.

Acknowledgements

References

1 W. W. Nazaroff, Indoor bioaerosol dynamics, *Indoor Air*, 2016, **26**, 61–78.

2 D. Meheust, P. L. Cann, G. Reboux, L. Millon and J.-P. Gangneux, Indoor fungal contamination: health risks and measurement methods in hospitals, homes and workplaces, *Crit. Rev. Microbiol.*, 2013, **40**, 248–260.

3 M. K. Ijaz, B. Zargar, K. E. Wright and J. R. Rubino, Generic aspects of the airborne spread of human pathogens indoors and emerging air decontamination technologies, *Am. J. Infect. Control*, 2016, **44**, S109–S120.

4 V. Navale, K. R. Vamkudoth, S. Ajmera and V. Dhuri, Aspergillus derived mycotoxins in food and the environment: prevalence, detection, and toxicity, *Toxicol. Rep.*, 2021, **8**, 1008–1030.

5 K. Shale and J. F. R. Lues, The etiology of bioaerosols in food environments, *Food Rev. Int.*, 2007, **23**, 73–90.

6 H. Mbareche, L. Morawska and C. Duchaine, On the interpretation of bioaerosol exposure measurements and impacts on health, *J. Air Waste Manage. Assoc.*, 2019, **69**, 789–804.

7 J. A. Huffman, A. E. Perring, N. J. Savage, B. Clot, B. Crouzy, F. Tummon, O. Shoshanim, B. Damit, J. Schneider, V. Sivaprakasam, M. A. Zawadowicz, I. Crawford, M. Gallagher, D. Topping, D. C. Doughty, S. C. Hill and Y. L. Pan, Real-time sensing of bioaerosols: review and current perspectives, *Aerosol Sci. Technol.*, 2020, **54**, 465–495.

8 Z. Suchorab, M. Frąc, Ł. Guz, K. Oszust, G. Łagod, A. Gryta, N. B. Wielgus and J. Czerwiński, A method for early detection and identification of fungal contamination of building materials using e-nose, *PLoS One*, 2019, **14**, e0215179.

9 J. Degois, X. Simon, C. Bontemps, P. Leblond and P. Duquenne, Characterization of experimental complex fungal bioaerosols: impact of analytical method on fungal composition measurements, *Aerosol Sci. Technol.*, 2019, **53**, 146–159.

10 C. Calderon, E. Ward, J. Freeman and A. McCartney, Detection of airborne fungal spores sampled by rotating-arm and Hirst-type spore traps using polymerase chain reaction assays, *J. Aerosol Sci.*, 2002, **33**, 283–296.

11 K. Yoo, T. K. Lee, E. J. Choi, J. Yang, S. K. Shukla, S. Hwang and J. Park, Molecular approaches for the detection and monitoring of microbial communities in bioaerosols: a review, *J. Environ. Sci.*, 2017, **51**, 234–247.

12 Ł. Grewling, A. Frątczak, Ł. Kostecki, M. Nowak, A. Szymańska and P. Bogawski, Biological and chemical air pollutants in an urban area of central Europe: co-exposure assessment, *Aerosol Air Qual. Res.*, 2019, **19**, 1526–1537.

13 Y. Ai, H. Alali, Y. L. Pan, G. Videen and C. Wang, Single-particle optical-trapping Raman spectroscopy for the detection and identification of aerosolized airborne biological particles, *Meas. Sci. Technol.*, 2021, **32**, 055207.

14 A. Pietrodangelo, S. Pareti and C. Perrino, Improved identification of transition metals in airborne aerosols by SEM-EDX combined backscattered and secondary electron microanalysis, *Environ. Sci. Pollut. Res.*, 2014, **21**, 4023–4031.

15 M. Wentzel, H. Gorzawski, K. H. Naumann, H. Saathoff and S. Weinbruch, Transmission electron microscopical and aerosol dynamical characterization of soot aerosols, *J. Aerosol Sci.*, 2003, **34**, 1347–1370.

16 A. T. Lebedev, Mass spectrometry in identification of ecotoxicants including chemical and biological warfare agents, *Toxicol. Appl. Pharmacol.*, 2005, **207**, 451–458.

17 P. Purohit, F. J. Fortes and J. J. Laserna, Optical trapping as a morphologically selective tool for in situ LIBS elemental characterization of single nanoparticles generated by laser ablation of bulk targets in air, *Anal. Chem.*, 2021, **93**, 2635–2643.

18 A. Brostrøm, K. I. Kling, K. S. Hougaard and K. Mølhave, Complex aerosol characterization by scanning electron microscopy coupled with energy dispersive X-ray spectroscopy, *Sci. Rep.*, 2020, **10**, 9150.

19 A. Miura, R. Nakajima, S. Abe and N. Kitamura, Optical trapping-microspectroscopy of single aerosol microdroplets in air: supercooling of dimethylsulfoxide microdroplets, *J. Phys. Chem. A*, 2020, **124**, 9035–9043.

20 J. Guicheteau, S. Christesen, D. Emge and A. Tripathi, Bacterial mixture identification using Raman and surface-enhanced Raman chemical imaging, *J. Raman Spectrosc.*, 2010, **41**, 1632–1637.

21 V. Sivaprakasam and M. B. Hart, Surface-enhanced Raman spectroscopy for environmental monitoring of aerosols, *ACS Omega*, 2021, **6**, 10150–10159.

22 V. Gabbarini, R. Rossi, J. F. Ciparisse, A. Malizia, A. Divizia, P. D. Filippis, M. Anselmi, M. Carestia, L. Palombi, M. Divizia and P. Gaudio, Laser-induced fluorescence (LIF) as a smart method for fast environmental virological analyses: validation on Picornaviruses, *Sci. Rep.*, 2019, **9**, 12598.

23 A. Gery, A. Delanoe, N. Heutte, E. Chosson, J. Bonhomme and D. Garon, A novel qPCR based-method for detection and quantification of three recurrent species of Penicillium isolated from bioaerosols in mold-damaged homes, *J. Microbiol. Methods*, 2021, **186**, 106236.

24 J. L. Santarpia, S. R. Shumate and A. Haddrell, Laboratory study of bioaerosols: traditional test systems, modern approaches, and environmental control, *Aerosol Sci. Technol.*, 2020, **54**, 585–600.

25 C. Xie, C. Goodman, M. A. Dinno and Y.-Q. Li, Real-time Raman spectroscopy of optically trapped living cells and organelles, *Opt. Express*, 2004, **12**, 6207–6214.

26 Z. Gong, Y. L. Pan, G. Videen and C. Wang, Optical trapping-Raman spectroscopy (OT-RS) with embedded microscopy imaging for concurrent characterization and monitoring of physical and chemical properties of single particles, *Anal. Chim. Acta*, 2018, **10120**, 86–94.

27 F. Schulte, J. Mader, L. W. Kroh, U. Panne and J. Kneipp, Characterization of pollen carotenoids with in situ and high-performance thin-Layer chromatography supported resonant Raman spectroscopy, *Anal. Chem.*, 2009, **81**, 8426–8433.

28 F. Schulte, J. Lingott, U. Panne and J. Kneipp, Chemical characterization and classification of pollen, *Anal. Chem.*, 2008, **80**, 9551–9556.

29 J. Ding, Q. Dai, Y. Zhang, J. Xu, Y. Huangfu and Y. Feng, Air humidity affects secondary aerosol formation in different pathways, *Sci. Total Environ.*, 2021, **759**, 143540.

30 B. R. Bzdek, J. P. Reid and M. I. Cotterell, Open questions on the physical properties of aerosols, *Commun. Chem.*, 2020, **3**, 105.

31 S. M. Kinahan, M. S. Tezak, C. M. Siegrist, G. Lucero, B. L. Servantes, J. L. Santarpia, A. Kalume, J. Zhang, M. Felton, C. C. Williamson and Y. L. Pan, Changes of fluorescence spectra and viability from aging aerosolized E. coli cells under various laboratory-controlled conditions in an advanced rotating drum, *Aerosol Sci. Technol.*, 2019, **53**, 1261–1276.

32 Z. Gong, Y. L. Pan, G. Videen and C. Wang, Chemical reactions of single optically trapped bioaerosols in a controlled environment, *Aerosol Sci. Technol.*, 2019, **53**, 853–859.

33 U. K. Krieger, C. Marcolli and J. P. Reid, Exploring the complexity of aerosol particle properties and processes using single particle techniques, *Chem. Soc. Rev.*, 2012, **41**, 6631–6662.

34 W. Li, L. Shao, D. Zhang, C. U. Ro, M. Hu, X. Bi, H. Geng, A. Matsuki, H. Niu and J. Chen, A review of single aerosol particle studies in the atmosphere of East Asia: morphology, mixing state, source, and heterogeneous reactions, *J. Clean. Prod.*, 2016, **112**, 1330–1349.

35 A. Kalume, C. Wang, J. Santarpiac and Y. L. Pan, Liquid-liquid phase separation and evaporation of a laser-trapped organic-organic airborne droplet using temporal spatial-resolved Raman spectroscopy, *Phys. Chem. Chem. Phys.*, 2018, **20**, 19151.

36 E. J. Davis, A history of single aerosol particle levitation, *Aerosol Sci. Technol.*, 1997, **26**, 212–254.

37 S. Santesson and S. Nilsson, Airborne chemistry: acoustic levitation in chemical analysis, *Anal. Bioanal. Chem.*, 2004, **378**, 1704–1709.

38 A. Ashkin, Acceleration and trapping of particles by radiation pressure, *Phys. Rev. Lett.*, 1970, **24**, 156–159.

39 R. Hopkins, L. Mitchem, A. Ward and J. Reid, Control and characterisation of a single aerosol droplet in a single-beam gradient-force optical trap, *Phys. Chem. Chem. Phys.*, 2004, **6**, 4924–4927.

40 Z. Gong, Y. L. Pan, G. Videen and C. Wang, The temporal evolution process of fluorescence bleaching and Raman spectra from single solid particles optically-trapped in air, *Chem. Phys. Lett.*, 2017, **689**, 100–104.

41 C. Wang, Y. L. Pan, S. C. Hill and B. Redding, Photophoretic trapping-Raman spectroscopy for single pollens and fungal spores trapped in air, *J. Quant. Spectrosc. Radiat. Transfer*, 2015, **153**, 4–12.

42 K. Kong, P. Zhang, P. Setlow and Y.-Q. Li, Characterization of bacterial spore germination using integrated phase contrast microscopy Raman spectroscopy and optical tweezers, *Anal. Chem.*, 2010, **82**, 3840–3847.

43 J. Lin and Y.-Q. Li, Optical trapping and rotation of airborne absorbing particles with a single focused laser beam, *Appl. Phys. Lett.*, 2014, **104**, 101909.

44 T. Shoji, D. Sugo, F. Nagasawa, K. Murakoshi, N. Kitamura and Y. Tsuboi, Highly sensitive detection of organic molecules on the basis of a poly (N-isopropylacrylamide)

© 2022 The Author(s). Published by the Royal Society of Chemistry

Environ. Sci.: Atmos., 2022, **2**, 591–600 | 599

microassembly formed by plasmonic optical trapping, *Anal. Chem.*, 2017, **89**, 532–537.

45 B. Redding and Y. L. Pan, Optical trap for both transparent and absorbing particles in air using a single shaped laser beam, *Opt. Lett.*, 2015, **40**, 2798–2801.

46 C. Wang, Y. L. Pan and G. Videen, Optical trapping and laser-spectroscopy measurements of single particles in air: a review, *Meas. Sci. Technol.*, 2021, **32**, 102005.

47 Z. Gong, Y. L. Pan, G. Videen and C. Wang, Optical trapping and manipulation of single particles in air: principles, technical details, and applications, *J. Quant. Spectrosc. Radiat. Transfer*, 2018, **214**, 94–119.

48 L. Mitchem and J. P. Reid, Optical manipulation and characterisation of aerosol particles using a single-beam gradient force optical trap, *Chem. Soc. Rev.*, 2008, **37**, 756–769.

49 Z. Liang, Y. Chu, M. Gen and C. K. Chan, Single-particle Raman spectroscopy for studying physical and chemical processes of atmospheric particles, *Atmos. Chem. Phys.*, 2022, **22**, 3017–3044.

50 C. Wang, Z. Gong, Y. L. Pan and G. Videen, Laser pushing or pulling of absorbing airborne particles, *Appl. Phys. Lett.*, 2016, **109**, 011905.

51 M. L. Laucks, G. Roll, G. Schweiger and E. J. Davis, Physical and chemical (Raman) characterization of bioaerosols-pollen, *J. Aerosol Sci.*, 2000, **31**, 307–319.

52 Z. Movasaghi, S. Rehman and I. U. Rehman, Raman spectroscopy of biological tissues, *Appl. Spectrosc. Rev.*, 2007, **42**, 493–541.

53 F. R. Hilsamar and P. H. R. Samuel, Raman spectroscopy techniques for the detection of biological samples in suspensions and as aerosol particles: a review, *Sens. Imaging*, 2012, **13**, 1–25.

54 K. Czamara, K. Majzner, M. Z. Pacia, K. Kochan, A. Kaczor and M. Baranska, Raman spectroscopy of lipids: a review, *J. Raman Spectrosc.*, 2015, **46**, 4–20.

55 C. Zhu, J. Farah, M. Choel, S. Gosselin, M. Baroudi, D. Petitprez and N. Visez, Uptake of ozone and modification of lipids in Betula pendula pollen, *Environ. Pollut.*, 2018, **242**, 880–886.

56 F. Cataldo, On the action of ozone on proteins, *Polym. Degrad. Stab.*, 2003, **82**, 105–114.

57 F. J. Hidalgo and R. Zamora, Formation of phenylacetic acid and benzaldehyde by degradation of phenylalanine in the presence of lipid hydroperoxides: new routes in the amino acid degradation pathways initiated by lipid oxidation products, *Food Chem.*, 2019, **2**, 100037.